www.czasopisma.pan.pl PAN POLSKA AKADEMIA NAUK www.journals.pan.pl

Arch. Min. Sci. **65** (2020), 2, 299-315

Electronic version (in color) of this paper is available: http://mining.archives.pl

DOI 10.24425/ams.2020.133194

HONGJUN GUO[1], MING JI[2*], WEISHENG ZHAO[3]

ROADWAY SUPPORT DESIGN BASED ON IN-SITU STRESS AND ITS ASYMMETRICAL DISTRIBUTIONS IN A COAL MINE

Through in-situ stress measurements, stress data were obtained from an auxiliary transportation roadway in a coal mine in Shanxi Province, China. Based on the principles of elastic mechanics and using a generalized plane strain model, the mechanical effects of the in-situ stresses on an idealized roadway were calculated and the distributions of stresses, displacements, and plastic zones determined. Building on this model, the vulnerable zones in the roadway cross section were identified. Ground support specifications were developed and during specification design, comprehensive consideration was given to factors affecting the stability of the rock surrounding the roadway. A scientific and reasonable support scheme was put forward. Practical experience in the coal mine shows the normal forces of anchor bolt and cable, the minimal convergence of roof to floor, and a generally good support in the auxiliary transportation roadway. The support should ensure safe production during its service life. This study provides a new method for designing roadway support systems that can be particularly valuable for high-stress roadways.

Keywords: in-situ stress; the stress in the rock surrounding roadway; the displacement in the rock surrounding roadway; the plastic zone in the rock surrounding roadway; support parameters

1. Introduction

Instability in the rock surrounding roadways is the result of stress; in-situ stress is a natural phenomenon that cannot be eliminated in underground mines. When mines become deeper, the in-situ stresses can cause rock deformation and failure and roadway instability increases [1].

[1] JIANGSU VOCATIONAL INSTITUTE OF ARCHITECTURAL TECHNOLOGY, XUZHOU, 221116, CHINA; CHINA UNIVERSITY OF MINING & TECHNOLOGY, STATE KEY LABORATORY OF COAL RESOURCES AND SAFE MINING, XUZHOU 221116, CHINA

[2] CHINA UNIVERSITY OF MINING & TECHNOLOGY, KEY LABORATORY OF DEEP COAL RESOURCE MINING, MINISTRY OF EDUCATION OF CHINA; SCHOOL OF MINES; XUZHOU, 221116, CHINA

[3] INSTITUTE OF MINING ENGINEERING, GUIZHOU INSTITUTE OF TECHNOLOGY, GUIYANG 550003, CHINA

* Corresponding author: jiming@cumt.edu.cn

Therefore, to guarantee safe production in mines, it is essential to understand the relationship between in-situ stresses and the rock surrounding the roadways.

Zheng used a generalized plane strain model to derive a series of expressions for stress and displacement in the volume of rock around a roadway [2]. Lu et al. analyzed the influence of the angle between maximum horizontal stress and the roadway's axis on stress and displacement distributions in the rock surrounding a roadway [3]. In addition, Chen discussed how maximum horizontal principal stress markedly influences roadway layout [4]. With the aid of numerical simulations, Xiao et al. analyzed surrounding rock stability in terms of the angular relationship between the orientation of the axis of roadways driven in thick coal seams and the direction of the horizontal principal stress [5]. Liu derived an equation for quantifying the influence of in-situ stress on the stability the rock surrounding a roadway and analyzed the distribution of stress and displacement in the rock surrounding deep roadways [6].

Some studies have explored the stability of the rock around roadways using numerical simulations of the angles between the roadways' axes and horizontal tectonic stresses, and made recommendations for practical roadway layouts and support schemes [7-11]. Combining numerical with physical simulations, Gou et al. analyzed the influence of horizontal stress on roadway stability Gou and coworkers considered the roof and floor of a roadway under significant horizontal stress to be a priority for stability control [12]. Zhao et al. investigated the influence of principal stress on the stability of surrounding rock at roadway intersections and found that near the intersection, the primary axis of the principal stress is deflected and its direction changes from horizontal to vertical [13,14].

The stability in the rock surrounding roadway is the result of the comprehensive action of geological factors, construction disturbance and technical conditions [15]. However, published studies on the relationship between in-situ stress and the stability of the rock surrounding roadways have mainly focused on the angle between the completely horizontal, relatively large principal stress and the roadway's axis. But in underground mines, there is commonly an angle between the "horizontal" principal stress and a true horizontal plane. Clearly, the studies mentioned above have limitations and the horizontal stress-roadway axis problem needs further investigation.

2. Engineering description

Fig. 1 shows the layout of an auxiliary transportation roadway in a coal mine in Shanxi Province, China. The roadway was excavated along the floor of the #3 coal seam with a buried depth of 450~550 m and is rectangular in cross section, 5.84 m high and 4.37 m wide. The parameters of the coal seam and its roof and floor are shown in Fig. 2 and Table 1.

TABLE 1

The mechanical parameters of rock surrounding roadway

Content	Compressive strength /MPa	Tensile strength /MPa	Elasticity modulus /GPa	Poisson's ratio	Cohesion /MPa	Internal friction angle /°
Mudstone	22.94	1.5	34.86	0.25	3.74	33.6
#3 coal	9.49	1.12	10.53	0.27	2.12	32.4
Sandstone	58.46	3.48	58.16	0.21	9.24	38.6

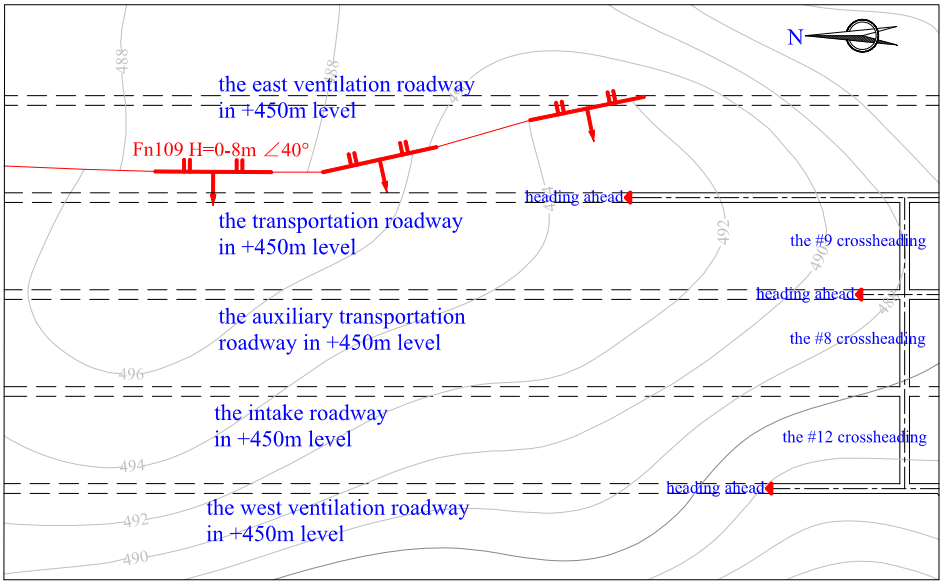

Fig. 1. Layout of an auxiliary transportation roadway in a coal mine in Shanxi Province, China

To obtain data on the in-situ stresses near the auxiliary transportation roadway, those measurement methods extensively used are compared (Table 2). And it has been demonstrated that the stress relief method is the most widespread and effective of the three methods [16-18]. Combined with the coal mine's actual conditions, it was also considered to be the most appropriate. When selecting the positions, it is critical to avoid the influences of geologic-structures and engineering disturbance. In view of the current conditions of the roadway and chamber, two stress measurement points were chosen. Point KD1 was located in the #8 drill station on the auxiliary transportation roadway (auxiliary 8), Point KD2 was located in the middle of the #8 crossheading between the intake roadway and the auxiliary transportation roadway (Fig. 3).

TABLE 2

Summary of the popular measurement methods for in-situ rock stress

Measurement method	Advantage	Disadvantage	Application scope
The stress relief method	High accuracy	Limited measurement points and potential technical difficulty	The existing roadway and chamber
The hydraulic fracturing method	Simple equipment, convenient operation, great representativeness, strong adaptability and big depth	Low accuracy, high cost, and bad direction of principal stress	Larger scope
The acoustic emission method	Low labor intensity, high integrity of study area, and repeatable measurement	Limited application scope and low accuracy	High strength brittle rock

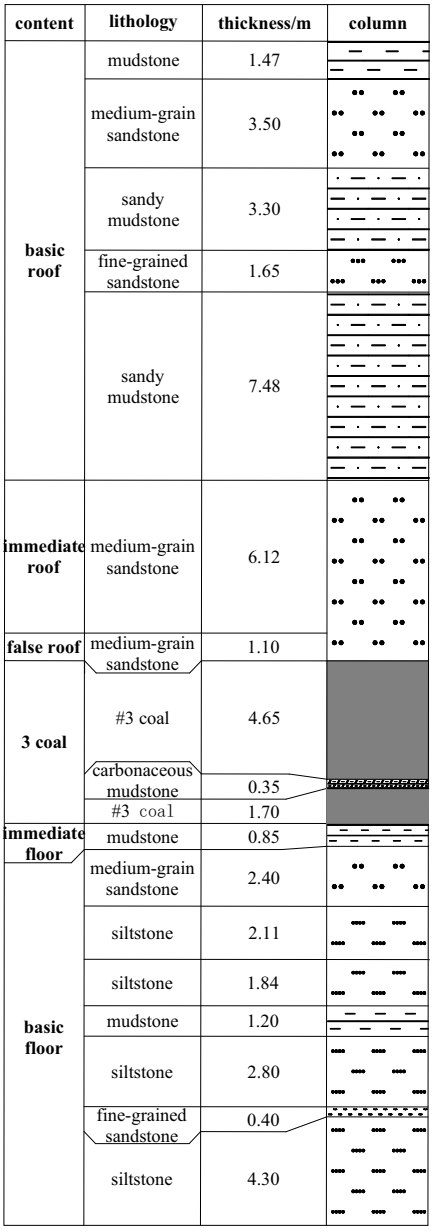

Fig. 2. Stratigraphic column showing the units above and below the #3 coal seam

Fig. 4 shows the diameter and length of the two bore holes and the coal petrography. The rock quality designation (RQD) for the core taken from the hole drilled at KD1 was 67%, the RQD for the core from the hole drilled at KD2 was 79%. These RQD's indicate good rock quality. The in-situ stress measurements are shown in Table 3.

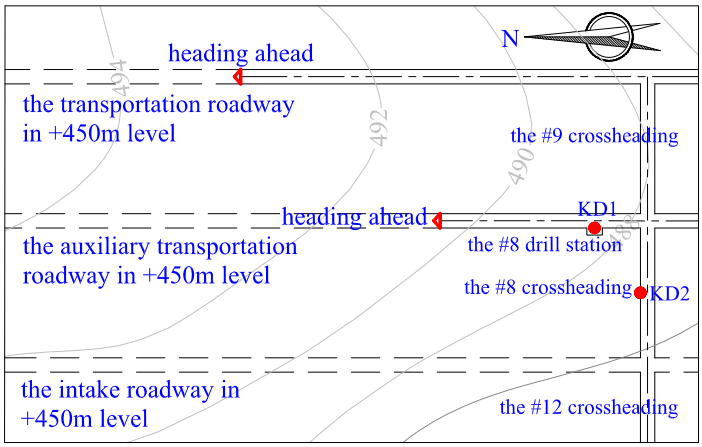

Fig. 3. Map showing the locations of the two in-situ stress measurement points

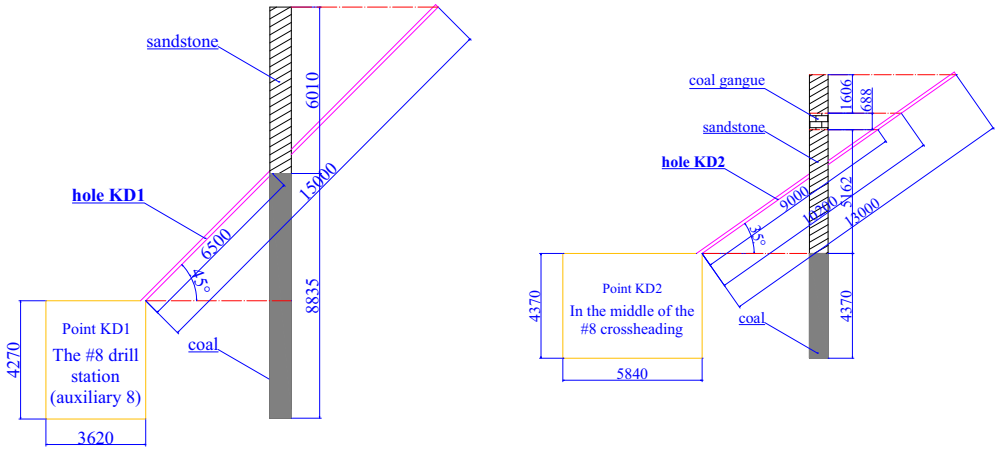

(a) KD1 (b) KD2

Fig. 4. Core hole statistics and coal and coal petrology for holes KD1 and KD2 (Unit: mm)

TABLE 3

In-situ stress measurements

Measurement station	Stress	Stress value / MPa	Direction angle / °	Dip angle / °
Point KD1 The #8 drill station (auxiliary 8)	σ_1	18.9	N31.55E	8.9
	σ_2	13.4	N222.5E	80.91
	σ_3	10.5	N121.79E	1.67
Point KD2 In the middle of the #8 crossheading	σ_1	18.8	N26.75E	5.98
	σ_2	13.6	N216.5E	83.93
	σ_3	10.9	N116.87E	1.04

Table 3 shows that the horizontal principal stress is the maximum ($\sigma_H > \sigma_v > \sigma_h$) and plays a dominant action in the stress field. Moreover, due to a large average ratio of 1.76 between the maximum horizontal principal stress and the minimum horizontal principal stress, the shear stress consisting of the above two horizontal stress has led to conditions favorable for the deformation and instability of the rock surrounding roadway. Therefore, the in-situ stress is a very important factor for support parameters design and surrounding rock control in the process of roadway construction.

3. Influence of in-situ stress on the stability of the rock surrounding roadway

3.1. Modeling

The in-situ stress measured by the hollow inclusion stress relief method, whose direction is arbitrary and different from the geodetic coordinate system, can not be directly used for mechanical analysis of the rock surrounding roadway. And it needs to be converted into a cylindrical coordinate system established along the roadway axis [6]. The specific steps are as follows:

(1) As shown in Fig. 5(a), by the tensor transformation method between the spatial relationship of the coordinate system and the stress component, the transformation from the principal stress coordinate system of $o_1x_1y_1z_1$ to the coordinate system of $o_2x_2y_2z_2$ is completed by using Eqs. (1).

$$B = L_{12} A L_{12}^{T} \tag{1}$$

where:

B — is the stress component matrix in the coordinate system of $o_2x_2y_2z_2$,

$$B = \begin{bmatrix} \sigma_{x_2} & \tau_{x_2y_2} & \tau_{x_2z_2} \\ \tau_{y_2x_2} & \sigma_{y_2} & \tau_{y_2z_2} \\ \tau_{z_2x_2} & \tau_{z_2y_2} & \sigma_{z_2} \end{bmatrix}$$

A — is the stress component matrix in the coordinate system of $o_1x_1y_1z_1$,

$$A = \begin{bmatrix} \sigma_3 & 0 & 0 \\ 0 & \sigma_1 & 0 \\ 0 & 0 & \sigma_2 \end{bmatrix}$$

L_{12} — is the direction cosine matrix of the angles (α, β and γ) consisting of corresponding axis in the coordinate systems of $o_2x_2y_2z_2$ and $o_1x_1y_1z_1$,

$$L_{12} = \begin{bmatrix} l_1 & m_1 & n_1 \\ l_2 & m_2 & n_2 \\ l_3 & m_3 & n_3 \end{bmatrix}$$

(2) As shown in Fig. 5(b), the stress component in the coordinate system of $o_2x_2y_2z_2$ is transformed to the coordinate system of $o_3x_3y_3z_3$, and the corresponding tensor matrix transformation is

$$C = L_{23} B {L_{23}}^T \tag{2}$$

where

C — is the stress component matrix in the coordinate system of $o_3x_3y_3z_3$,

$$C = \begin{bmatrix} \sigma_{x_3} & \tau_{x_3y_3} & \tau_{x_3z_3} \\ \tau_{y_3x_3} & \sigma_{y_3} & \tau_{y_3z_3} \\ \tau_{z_3x_3} & \tau_{z_3y_3} & \sigma_{z_3} \end{bmatrix}$$

L_{23} — is the direction cosine matrix of the angles (0, φ and φ) consisting of corresponding axis in the coordinate systems of $o_3x_3y_3z_3$ and $o_2x_2y_2z_2$,

$$L_{23} = \begin{bmatrix} 1 & 0 & 0 \\ 0 & \cos\varphi & -\sin\varphi \\ 0 & \sin\varphi & \cos\varphi \end{bmatrix}$$

Combining Eqs. (1) and Eqs. (2), three principal stresses can be transformed to the space rectangular coordinate system composed of a section of the roadway and its axial direction in any direction, namely

$$C = L_{23} L_{12} A {L_{12}}^T {L_{23}}^T \tag{3}$$

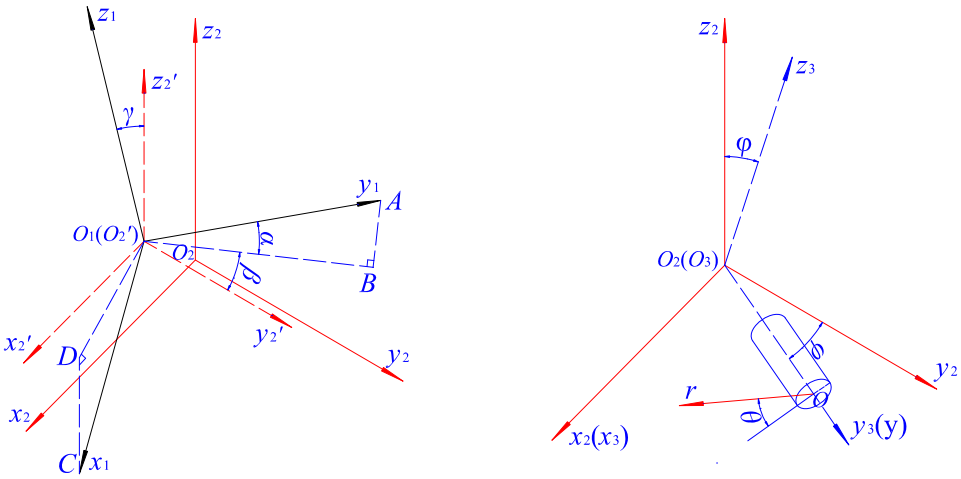

(a) (b)

Fig. 5. The spatial stress convertion model

(3) By substituting Eqs. (3) into generalized plane strain model Eqs. (4) and Eqs. (5), the stress and displacement in the rock surrounding circular roadway can be obtained [2].

$$\left.\begin{aligned}
\sigma_r &= \frac{\sigma_x+\sigma_z}{2}\left(1-\frac{a^2}{r^2}\right)+\frac{\sigma_x-\sigma_z}{2}\left(1+\frac{3a^4}{r^4}-\frac{4a^2}{r^2}\right)\cos 2\theta \\
&\quad +\tau_{xz}\left(1+\frac{3a^4}{r^4}-\frac{4a^2}{r^2}\right)\sin 2\theta \\
\sigma_\theta &= \frac{\sigma_x+\sigma_z}{2}\left(1+\frac{a^2}{r^2}\right)-\frac{\sigma_x-\sigma_z}{2}\left(1+\frac{3a^4}{r^4}\right)\cos 2\theta-\tau_{xz}\left(1+\frac{3a^4}{r^4}\right)\sin 2\theta \\
\sigma_{y'} &= \sigma_y-\mu\left[2(\sigma_x-\sigma_z)\cos 2\theta+4\tau_{xz}\sin 2\theta\right]\frac{a^2}{r^2} \\
\tau_{r\theta} &= -\frac{\sigma_x-\sigma_z}{2}\left(1-\frac{3a^4}{r^4}+\frac{2a^2}{r^2}\right)\sin 2\theta+\tau_{xz}\left(1-\frac{3a^4}{r^4}+\frac{2a^2}{r^2}\right)\cos 2\theta \\
\tau_{ry} &= (\tau_{xy}\cos\theta+\tau_{yz}\sin\theta)\left(1-\frac{a^2}{r^2}\right) \\
\tau_{\theta y} &= (-\tau_{xy}\sin\theta+\tau_{yz}\cos\theta)\left(1+\frac{a^2}{r^2}\right)
\end{aligned}\right\} \tag{4}$$

where

$\begin{bmatrix} \sigma_r & \tau_{r\theta} & \tau_{ry} \\ \tau_{\theta r} & \sigma_\theta & \tau_{\theta y} \\ \tau_{yr} & \tau_{y\theta} & \sigma_{y'} \end{bmatrix}$ — is the stress component matrix around the roadway in a cylindrical coordinate system;

θ — is the angle between the radial direction of the plane of *xoy* and the axis *ox*;

a — is the radius of circular roadway or the equivalent radius of non-circular roadway;

r — is the distance from any point in the radial direction of circular roadway to the origin *O*.

$$\left.\begin{aligned}
u &= \frac{1+\mu}{E}\frac{a^2}{2r}\left\{(\sigma_x+\sigma_z)+(\sigma_x-\sigma_z)\left[-\frac{a^2}{r^2}+4(1-\mu)\right]\cos 2\theta\right. \\
&\quad \left.+\frac{\tau_{xz}a^2}{r^2}\left[-\frac{a^2}{r^2}+4(1-\mu)\right]\sin 2\theta\right\} \\
v &= -\frac{1+\mu}{E}\frac{a^2}{2r}\left[(\sigma_x-\sigma_z)\sin 2\theta-2\tau_{xz}\cos 2\theta\right]\left[\frac{a^2}{r^2}+2(1-2\mu)\right] \\
w &= \frac{2(1+\mu)}{E}\frac{a^2}{r^2}(\tau_{yz}\sin\theta+\tau_{xy}\cos\theta)
\end{aligned}\right\} \tag{5}$$

where

$\begin{bmatrix} u \\ v \\ w \end{bmatrix}$ — is the displacement matrix around the roadway in a cylindrical coordinate system;

μ — is poisson's ratio;
E — is elastic modulus.

The distance within which the rock near a roadway can be deformed is generally three to five times the roadway's equivalent radius [19,20], namely 10.95-18.25 m. Because the magnitude and direction of the stress measured at the two measurement points are similar and Point KD1 is located in the auxiliary transportation roadway, we selected the in-situ stress data from Point KD1 in the range of 15 m as the data to use for the following calculations and analysis (Table 3). Previous studies have shown that the stresses in the rock surrounding a roadway are not evenly distributed; they change radially around the roadway and with their distance from the roadway. The magnitude and direction of a stress at any position near the roadway was determined by changing the value of θ in the above equations [21].

3.2. Stress distribution in the rock surrounding roadway

By substituting the relevant parameters into Eqs. (4), we calculated the stresses in the volume of rock extending 15 m from the roadway assuming that the roadway was unsupported (Figs. 6, 7).

Figs 6 and 7 show that the stresses change radially around the roadway. The stresses are extremely varied in the zone 0-3 m from the roadway. Beyond that there is a transitional zone for 3-5 m and then the stress variability is much reduced in a zone that extends from 5-10 m. At distances greater than 10 m from the roadway, the stresses appear to be stable. Circumferential stress dominates in the rock near the roadway but stress gradually decreases as one looks deeper into the roadway walls. In contrast, the radial stress is zero at the roadway itself but gradually increases as the depth in the walls increases. The axial stress variations are not particularly significant radially around the roadway. Compared with the normal stress, the shear stress is

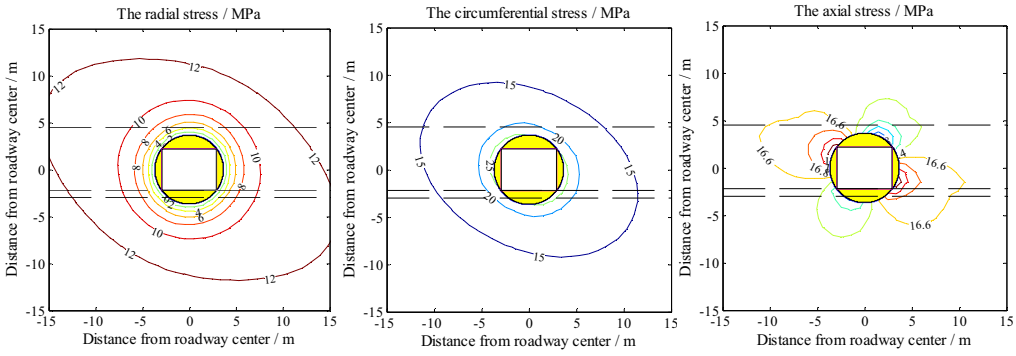

Fig. 6. Contours showing the distribution of stresses for 15 m in the rock surrounding the roadway

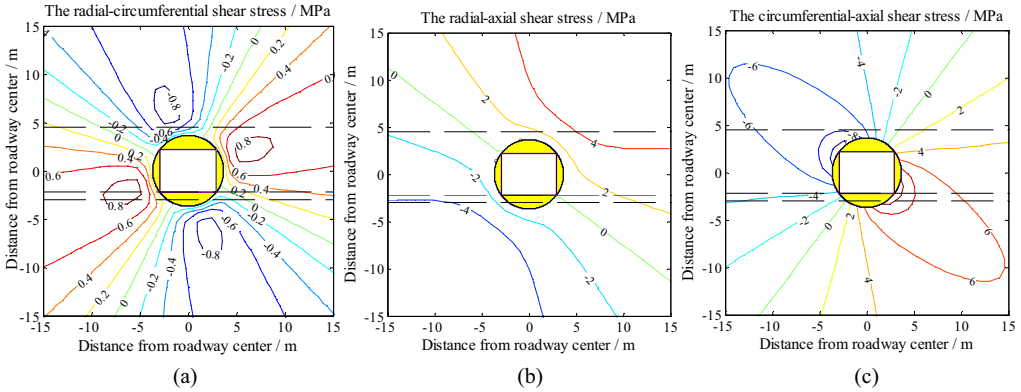

Fig. 7. Contours showing the distribution of shear stresses for 15 m in the rock surrounding the roadway

relatively low. The radial variation in the shear stress at any fixed distance from the roadway is essentially zero but this stress increases as one moves from the deep surrounding rock towards the roadway. The shear stress in the radial-axial plane gradually increases but the shear stress in the circumferential-axial plane gradually decreases. However, there is considerable directionality at different positions of the roadway.

By applying the principles of elastic mechanics, the values of the above six stress components were used to calculate the principal stress at different points in the rock surrounding the roadway. These principal stresses are shown in Fig. 8.

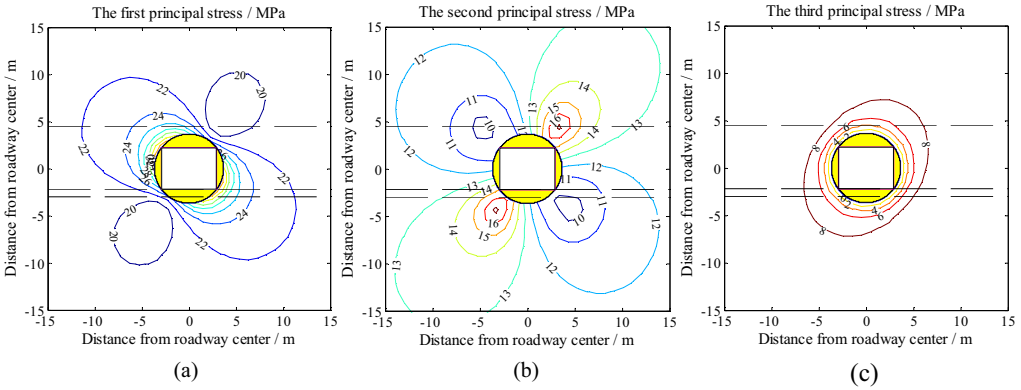

Fig. 8. Contours showing third principal stress deep in the rock surrounding the roadway

Similarly, the same intervals for the extent of stress variation described above are obtained in Fig. 8. The first principal stress on the roadways floor, walls, and roof is approximately 30 MPa and the magnitude of this stress decreases into the rock away from the roadway. The stress gradients differ along different radial directions around the roadway cross section and these variations can be roughly divided into variations in the two directions of the roadway's diagonal. The second principal

stress is relatively small and increases as the radial distance from roadway increases in the two directions of the roadway's diagonals. The third principal stress is the smallest; it gradually increases at greater distances but its gradient does not show any significant differences around the roadway.

3.3. Displacement distribution in the rock surrounding roadway

Similar to the way in which stress distributions were calculated, the relevant parameters were substituted into an equation, Eq. (5), to obtain the displacements for the rock within 15 m of the (unsupported) roadway. The results of the calculations are shown in Fig. 9.

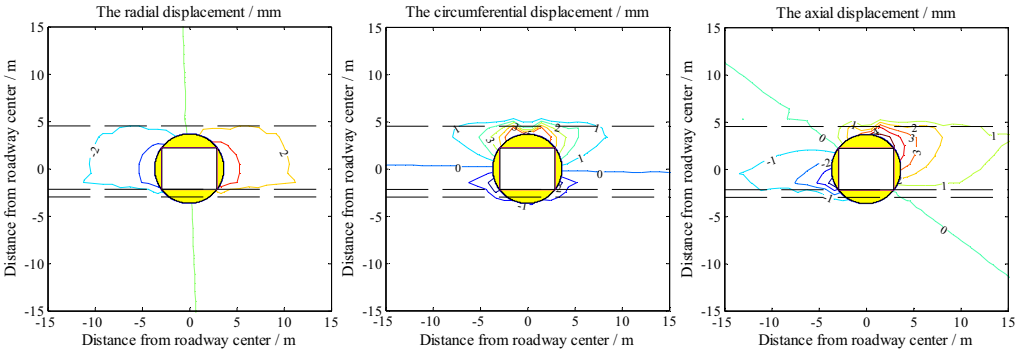

Fig. 9. Contours showing the distribution of displacements in the rock within 15 m of the unsupported roadway

Fig. 9 shows that there is little variation in displacement in the rock surrounding the roadway. The displacement variation intervals are similar to those obtained for the stresses. The radial and axial displacements decrease as distance from the roadway increases and both of them fall to zero more than a distance of around 10 m. In general, the displacements are not affected by any radial variations.

3.4. Plastic zone distribution in the rock surrounding roadway

According to the Mohr-Coulomb failure criterion [22-25], when the actual principal stress σ_1 and the theoretical stress σ_1' meet, Eq. (6), below, plastic failure occurs in the material. Using the relevant parameters again, the boundaries of the plastic zone in the rock adjacent to the roadway were calculated and the plastic zone is illustrated Fig. 10.

$$\sigma_1 > \sigma_1' = \sigma_3 \frac{1+\sin\varphi}{1-\sin\varphi} + 2c\frac{\cos\varphi}{1-\sin\varphi} \tag{6}$$

where

$\sigma_1(\sigma_3)$ — is the first (third) principal stress;
φ — is the internal friction angle;
c — is the cohesion.

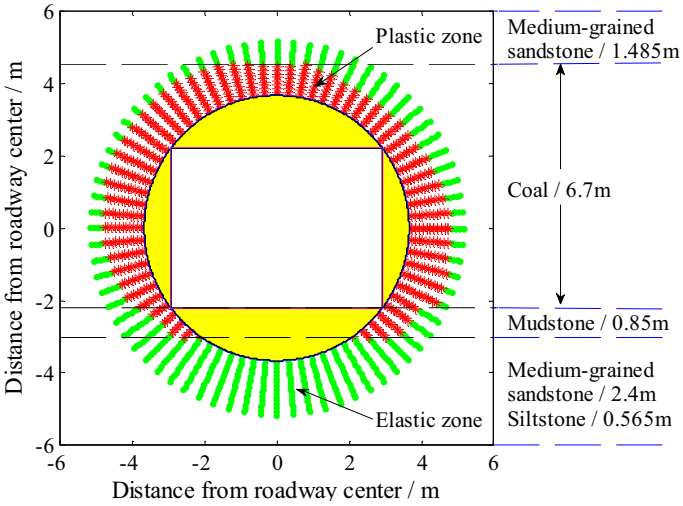

Fig. 10. Illustration showing the distribution of the plastic zone adjacent to the roadway

Fig. 10 shows that the plastic zone is asymmetrically distributed around the circumference of the tube-like idealized circular roadway to the depth of 1.3 m. Assuming that the volume of rock between the circular walls of the idealized roadway and the walls of the actual rectangular roadway are in the plastic zone, then the plastic zone would extend 2.33 m above in the roof and nearly 2 m into the sidewalls of the actual rectangular roadway. During excavation, as the roadway is advanced, the plastic zone in the roof is much thicker than the plastic zone in the floor. This is very important in terms of roof support management and must be considered when choosing roadway support bolt lengths.

4. Roadway support design based on in-situ stress

Taking the in-situ stress into account, the following issues need to be addressed when choosing roadway support parameters:

(1) The stress and displacement variations in the rock surrounding the roadway.
(2) The stress levels in the rock within the range of anchor bolt and cable supports. This is especially true for rock that will anchor support bolts; the possibility that narrow zones of high stress exist should also be considered.
(3) The distribution and thickness of the plastic zones in the rock surrounding the roadway.

After considering the issues described above, 2.4 m sidewall and 2.6 m roof bolt lengths were selected for the auxiliary transportation roadway [1,26]. The final support parameters and support section are shown in Fig. 11.

To verify the effectiveness of the supports, the force of anchor bolt and cable and the displacement in the rock surrounding roadway were monitored by hydraulic pillows and cross point method, and the monitoring stations were installed on the site (Figs 12a and 13a) [27,28]. The monitoring results are shown in Figs 12b-d and 13b-d.

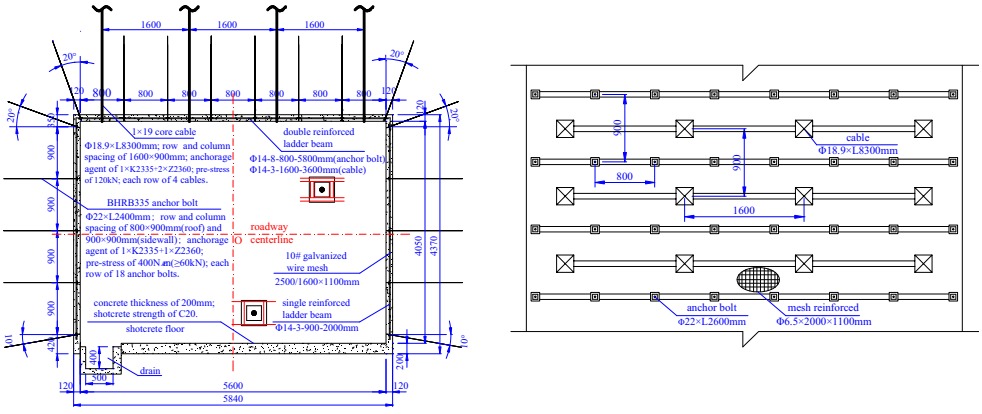

(a) (b)

Fig. 11. Cross section showing the support scheme for the auxiliary transportation roadway

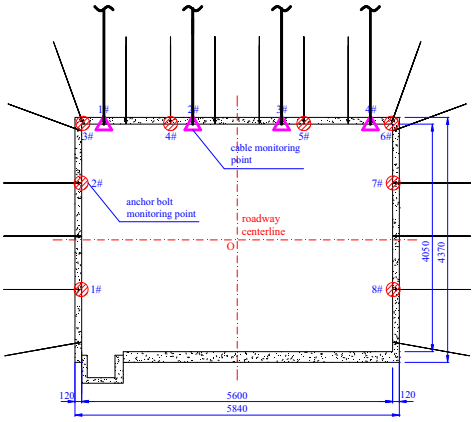

(a) layout of monitoring station

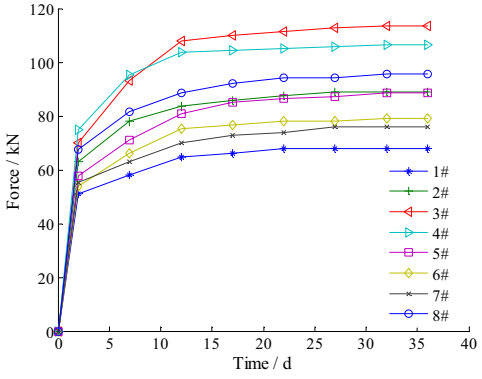

(b) anchor bolt

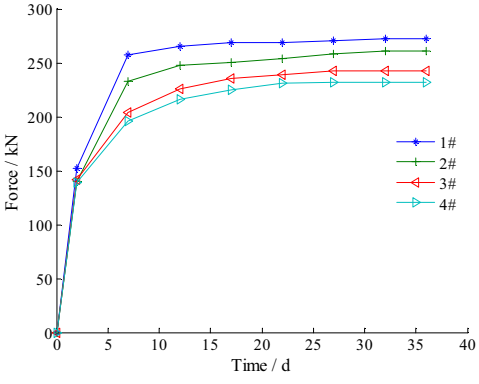

(c) cable

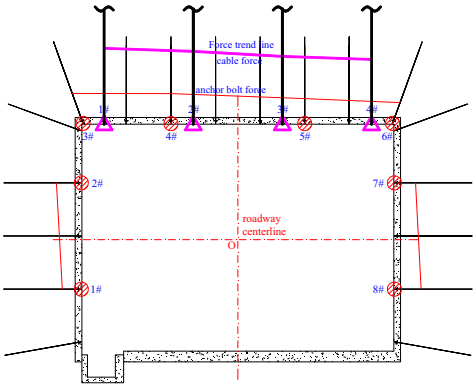

(d)

Fig. 12. Monitoring station results for anchor bolt and cable force

The roof bolt has a larger force than the sidewall bolt. The maximum force of the roof bolts is 105 kN whereas that of the sidewall bolts is 78 kN. The maximum (average) force accounts for 89.4% (70.5%) of the yield load of the bolts. The force imposed on the anchor cable is relatively uniform and the maximum (average) imposed force accounts for 56% (51.8%) of the cable's breaking strength. Both the anchor bolts and the cable are performing very well and have a surplus of support capacity and can meet the support requirements. The forces imposed on the supports are not uniform. There is a relatively large force on the left shoulder indentation and the right foot bottom (Fig. 12d). This is consistent with the above-mentioned stress patterns and the distribution of the plastic zones in the rock. It is a physical example of the different forces in the surrounding rock at different positions around the roadway. These stress patterns are predominantly influenced by the maximum principal stress.

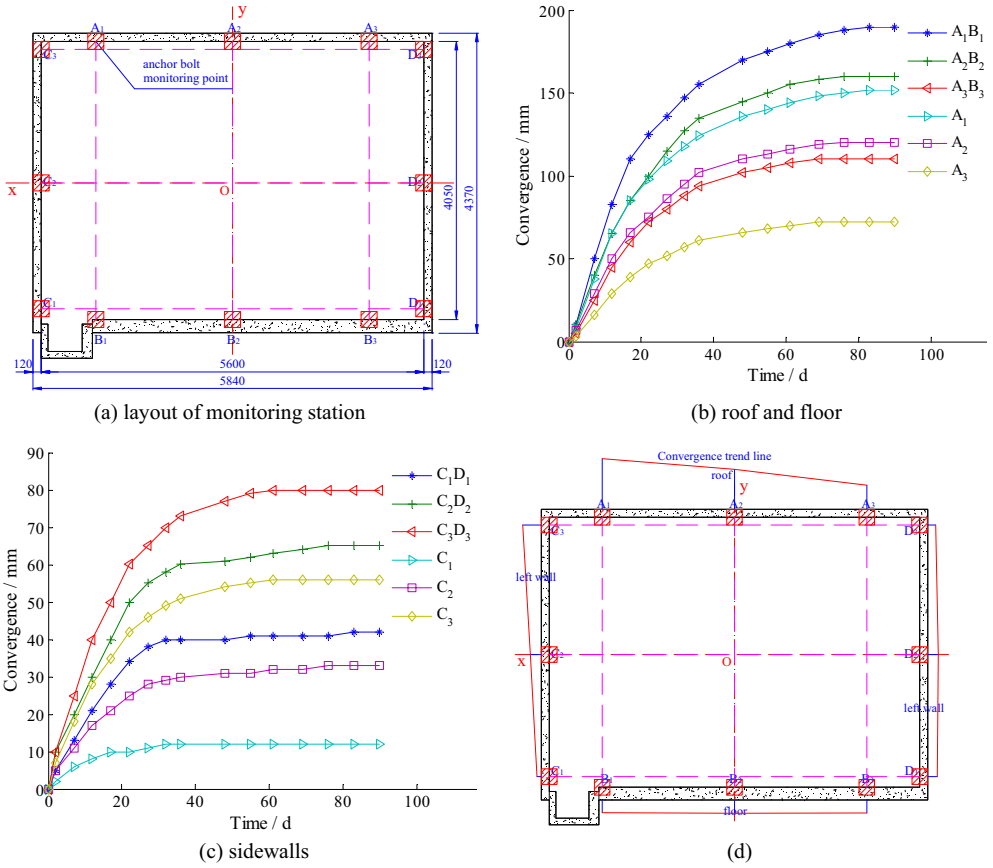

(a) layout of monitoring station (b) roof and floor

(c) sidewalls (d)

Fig. 13. Monitoring station results for roadway roof–floor and sidewall convergence

The convergence in the roadway is relatively small. The roof to floor convergence is no more than 200 mm, the sidewall convergence is less than 100 mm, and the floor heave only about 40 mm. The convergence is relatively large at point A_1 in the roof and point C_3 in the sidewall

(Fig. 13); that is, the convergence is greatest in the left shoulder indentation. Generally, the support is satisfactory and the surrounding rock is under effective control. The largest convergences are taking place in the sections of roadway with the thickest plastic zones (Fig. 13d), and their overall distribution is generally consistent with the direction of the dominant stress in the surrounding rock.

5. Conclusions

Using an analysis of in-situ stresses, this study presents a theoretical analysis on stress and displacement patterns and the distribution of plastic zones around an idealized roadway in an underground mine. The study also proposes parameters for roadway support bolts and cables. The conclusions are:

(1) The in-situ stresses near the auxiliary transportation roadway studied are dominated by the horizontal principal stress. The magnitude of the maximum horizontal stress is 18.9 MPa and there is an angle of 31.55° between the stress direction and the roadway axis.

(2) The stress and displacement in the rock surrounding roadway show considerable variation. These variations are quite severe in a 3 m zone adjacent to the roadway walls and roof, less sever in a transition zone that extends from 3 m to 5 m, and much reduced in an outermost zone between 5 m and 10 m. The rock greater than 10 m from the roadway appears to be stable. Circumferential stress is dominant in the rock close to the roadway and radial stress becomes dominant farther from the roadway but here is little variation in displacement. The stress and displacement variations are not the same along different radii on a vertical cross section through the roadway.

(3) The plastic deformation zone is asymmetrically distributed around the roadway. The surrounding rock 2.33 m immediately above the roof and within 2 m of the roadway sidewalls is in a plastic state. The extent of this plastic zone is important for decisions on bolt requirements and for roof management.

(4) Bolts and cables were installed for ground support and practice indicates that the support scheme, designed on the basis of in-situ stress measurements, is practical and sufficient. The maximum (and average) force on the anchor bolts is 89.4% (70.5%) of their yield strength and the maximum (and average) force on the anchor cable is 56% (51.8%) of its breaking load. The roof to floor convergence in the roadway is less than 200 mm, the sidewall convergence and floor heave are also minimal, and this should meet the requirements for safe production.

(5) The anchor bolt and cable force and the cross-sectional convergence of the roadway are closely related to the distribution of the plastic zone and the dominant stress in the surrounding rock. The positions of the anchor bolts that are sustaining larger forces and the locations of the rock that is being severely deformed are generally consistent with the direction of the dominant stress in this region.

Acknowledgments

This paper is supported by Guizhou Science and Technology Plan Project (Guizhou Science and Technology Cooperation Support [2019]2882, Guizhou Science and Technology Cooperation Foun-

dation [2018]1061, Guizhou Science and Technology Cooperation Platform Talents [2017]5789-12), Youth Science and Technology Talent Growth Project of Guizhou Education Department (Guizhou Education Combined KY Character [2017] 219), and the Fundamental Research Funds for the Central Universities (Grant No. 2017XKQY044).
We thank David Frishman, PhD, from Liwen Bianji, Edanz Group China (www.liwenbianji.cn/ac), for editing the English text of a draft of this manuscript.

References

[1] B.T. Shen, *Coal Mine Roadway Stability in Soft Rock: A Case Study*. Rock Mech. Rock Eng. (2014), DOI: 10.1007/s00603-013-0528-y.

[2] Y.T. Zheng, *Rock Mechanics of Elastoplastic Problems*. China Coal Industry Publishing House, Beijing (1988).

[3] Y. Lu, X.Z. Zou, C.Y. Liu, J.B. Bai, *Roadway Layout in Tectonic Stress Field*. J. Min. Safety Eng. (2008), DOI: 10.3969/j.issn.1673-3363.2008.02.004.

[4] D.H. Chen, X.Z. Hua, *Impact of In-situ Stress on Layout Direction of Deep Typical Gateways*. Chin. J. Undergr. Sp. Eng. (2018), DOI: CNKI:SUN:BASE.0.2018-04-034.

[5] T.Q. Xiao, G.H. Zhi, Z.G. Zhang, *Relationship Between Ground Stress Distribution and Roadway Stability in Deep Tectonic Region*. J. Min. Safety Eng. **30** (5), 659-664 (2013).

[6] H.Q. Liu, *MSc thesis, Study on the Relationship of the Ground Stress and Roadway Surrounding Rock Stability in Gucheng Coal Mine*. China University of Mining and Technology, Xuzhou, China (2014).

[7] G.Z. Xue, C. Gu, C, X.Q. Fang, T. Wei, *A Case Study on Large Deformation Failure Mechanism and Control Techniques for Soft Rock Roadways in Tectonic Stress Areas*. Sustainability. (2019), DOI: 10.3390/su11133510.

[8] H. Li, B.Q. Lin, Y.D. Hong, Y.B. Gao, W. Yang, T. Liu, R. Wang, Z.B. Huang, *Stress and Displacement Evolution Features of Opening Seam in Mine Cross Cut Based on Different In-Situ Rock Stress and Orientations*. Int. J. Min. Sci. Tech. (2017), DOI: 10.13199/j.cnki.cst.2017.10.015.

[9] Q.B. Meng, L.J. Han, W.G. Qiao, D.G. Lin, Y.X. Lv, *Research on Deep Soft Roadway Stability Based on In-site Geo-Stress Measurement*. Chin. J. Undergr. Sp. Eng. (2012), DOI: 10.1007/s11783-011-0280-z.

[10] C.D. Tian, H.B. Bai, *Impact Analysis of Roadway Size and Layout on Stability of Surrounding Rock*. Safety in Coal Mines (2015), DOI: 10.13347/j.cnki.mkaq.2015.08.064.

[11] B.H. Zhang, L.J. Han, G.L. Han, Y.N. Wang, *Study of 3D In-Situ Stress Measurement and Stability of Roadways in Depth*. Rock and Soil Mech. (2008), DOI:10.1016/S1872-5813(08)60033-X.

[12] P.F. Gou, S.J. Wei, S. Zhang, *Numerical Simulation of Effect of Horizontal Stresses at Different Levels on Stability of Roadways*. J. Min. Safety Eng. (2010), DOI: CNKI:SUN:KSYL.0.2010-02-002.

[13] W.S. Zhao, L.J. Han, Y.D. Zhang, *Study on the Change Law of Disturbance Principal Stress and the Stability of Surrounding Rock of Vertical Working Intersection*. J. Min. Safety Eng. (2015), DOI: 10.13545/j.cnki.jmse.2015.01.015.

[14] W.S. Zhao, L.J. Han, Z.N. Zhao, Q.B. Meng, H.Q. Liu, *Influence of Principal Stress on Surrounding Rock Stability of Roadway Intersection*. Rock and Soil Mech. (2015), DOI: 10.16285/j.rsm.2015.06.029.

[15] P. Małkowski, Z. Niedbalski, T. Majcherczyk, *Roadway Design Efficiency Indices for Hard Coal Mines*. Acta Geodyn Geomater. (2016), DOI: 10.13168/agg.2016.0002.

[16] F.D. Stacey, *The Measurement of Stress Effects in Rock Magnetism*. Dev. Solid Earth Geophy. (2013), DOI: 10.1016/B978-1-4832-2894-5.50094-X.

[17] Z.L. Sui, L. Qiao, X.S. Sun, *In-situ Stress Measurement by CSIRO Hollow Inclusion Cell in Yuyuan Mine*. Metal Mine (2009), DOI: CNKI:SUN:JSKS.0.2009-08-024.

[18] M.L. Wu, C.T. Liao, C.S. Zhang, M.Y. Ou, *Research on In-Situ Stress Measurement and Its Distribution Law in Hongtoushan Copper Mine*. Chin. J. Rock Mech. Eng. (Chin). (2004), DOI: 10.1007/BF02911033.

[19] C.W. Liu, L. Cao, S.X. Liu, *Method of "Equivalent Radius" for the Analyzing Rock Stress of High-buried Non-circular Underground Chambers*. Copper. Eng. (2010), DOI: 10.3969/j.issn.1009-3842.2010.01.001.

[20] G.C. Li, N. Zhang, C. Wang, N.C. Zhang, B.Y. Li, *Optimizing the Section Shape of Roadways in High Stress Ground by Numerical Simulation*. J. Chin. Univ. Min. Tech. (2010), DOI: 10.1016/S1876-3804(11)60004-9.

[21] S.Q. Yang, C. Miao, G. Fang, Y.C. Wang, B. Meng, Y.H. Li, H.W. Jing, *Physical Experiment and Numerical Modelling of Tunnel Excavation in Slanted Upper-Soft and Lower-Hard Strata*. Tunn. Undergr. Sp. Tech. (2018), DOI: 10.1016/j.tust.2018.08.049.

[22] W.G. Cao, M.H. Zhao, C.X. Liu, *Study on Rectified Method of Mohr-Coulomb Strength Criterion for Rock Based on Statistical Damage Theory*. Chin. J. Rock. Mech. Eng. (2005), DOI: 10.1007/s11769-005-0030-x.

[23] Y.D. Lin, M. Tu, *Resolving Analysis of Rock Plastic Zone in Round Roadway with Inhomogenous Stress Field*. Coal Sci. Tech. Mag. (2011), DOI: CNKI:SUN:META.0.2011-02-016.

[24] X.X. Yang, H.W. Jing, K.F. Chen, W.L. Wang, *Study on Influence Law of In-Situ Stress in Deep Underground Rocks on the Size of Failure Zone in Roadway*. J. Min. Safety Eng. **30** (4), 495-500 (2013).

[25] W.H. Zha, X.Z. Hua, D.H. Chen, *Quantitative Analysis of Plastic Region in Deep Buried Tunnel Based on In-Situ Stress Test*. J. Exp. Mech. (2013), DOI: CNKI:SUN:SYLX.0.2013-05-016.

[26] M.L. Zhang, Y.D. Zhang, *Stability Evaluation Method for Gateways in Closely Spaced Coal Seams and Surrounding Rock Control Technology*. Arab. J. Sci. Eng. (2018), DOI: 10.1007/s13369-018-3201-7.

[27] Z. Niedbalski, P. Małkowski, T. Majcherczyk, *Monitoring of Stand-and-Roof-Bolting Support: Design Optimization*. Acta Geodyn. Geomater. (2013), DOI: 10.13168/AGG.2013.0022.

[28] T. Majcherczyk, P. Małkowski, Z. Niedbalski, *Rock Mass Movements Around Development Workings in Various Density of Standing-and-Roof-Bolting Support*. J. Coal Sci. Eng. (Chin). (2008), DOI: 10.1007/s12404-008-0078-1.